JACS
JOURNAL OF THE AMERICAN CHEMICAL SOCIETY
pubs.acs.org/JACS
Article

High Efficiency Polymer Solar Cells with Efficient Hole Transfer at Zero Highest Occupied Molecular Orbital Offset between Methylated Polymer Donor and Brominated Acceptor

Chenkai Sun,[▽] Shucheng Qin,[▽] Rui Wang, Shanshan Chen, Fei Pan, Beibei Qiu, Ziya Shang, Lei Meng, Chunfeng Zhang, Min Xiao, Changduk Yang, and Yongfang Li*

Cite This: J. Am. Chem. Soc. 2020, 142, 1465−1474

Read Online

ACCESS | Metrics & More | Article Recommendations | Supporting Information

ABSTRACT: Achieving efficient charge transfer at small frontier molecular orbital offsets between donor and acceptor is crucial for high performance polymer solar cells (PSCs). Here we synthesize a new wide band gap polymer donor, PTQ11, and a new low band gap acceptor, TPT10, and report a high power conversion efficiency (PCE) PSC (PCE = 16.32%) based on PTQ11−TPT10 with zero HOMO (the highest occupied molecular orbital) offset ($\Delta E_{HOMO(D-A)}$). TPT10 is a derivative of Y6 with monobromine instead of bifluorine substitution, and possesses upshifted lowest unoccupied molecular orbital energy level (E_{LUMO}) of −3.99 eV and E_{HOMO} of −5.52 eV than Y6. PTQ11 is a derivative of low cost polymer donor PTQ10 with methyl substituent on its quinoxaline unit and shows upshifted E_{HOMO} of −5.52 eV, stronger molecular crystallization, and better hole transport capability in comparison with PTQ10. The PSC based on PTQ11−TPT10 shows highly efficient exciton dissociation and hole transfer, so that it demonstrates a high PCE of 16.32% with a higher V_{oc} of 0.88 V, a large J_{sc} of 24.79 mA cm^{-2}, and a high FF of 74.8%, despite the zero $\Delta E_{HOMO(D-A)}$ value between donor PTQ11 and acceptor TPT10. The PCE of 16.32% is one of the highest efficiencies in the PSCs. The results prove the feasibility of efficient hole transfer and high efficiency for the PSCs with zero $\Delta E_{HOMO(D-A)}$, which is highly valuable for understanding the charge transfer process and achieving high PCE of PSCs.

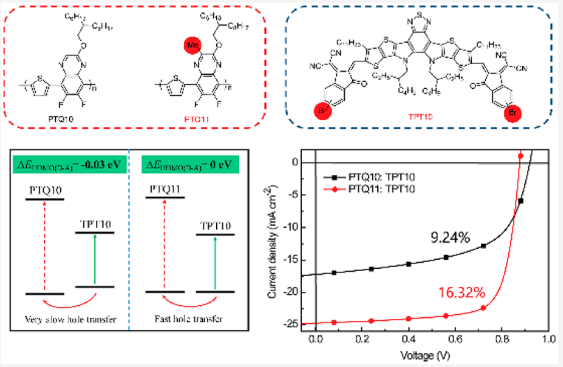

INTRODUCTION

Bulk-heterojunction polymer solar cells (PSCs), blending a p-type conjugated polymer as electron donor and an n-type organic semiconductor (n-OS) as electron acceptor for efficient exciton dissociation and charge carrier transfer,[1−3] have demonstrated considerable potential in utilizing renewable solar energy because of their intrinsic advantages of low cost fabrication by solution processing,[4−6] light weight,[7,8] and flexibility.[9,10] The photovoltaic power conversion efficiency (PCE) of single-junction PSCs has been gradually increased to over 15%[11−13] over the past years due to great innovations in efficient photovoltaic materials,[5,11,14−20] interface buffer layer materials,[21−25] active layer morphology optimization,[8,26,27] etc. And all-polymer solar cells that employ p-type conjugated polymer as donor and n-type conjugated polymer as acceptor have also achieved rapid development through the rational molecular structure optimization of photovoltaic materials and device engineering.[28] In addition, side-chain engineering[3,29] and fluorine substitution[20,30] have been widely used in the design of high performance photovoltaic materials for PSCs for tuning their electronic energy levels and aggregation properties.

High efficiency PSCs require the realization of high open-circuit voltage (V_{oc}), large short-circuit current density (J_{sc}), and high fill factor (FF) simultaneously. In the donor/acceptor (D/A) blends of efficient PSCs, the photovoltaic materials absorb photons to generate excitons, and the excitons diffuse to the D/A interface where they dissociate into a charge transfer (CT) state electron−hole pair under an extra driving force with the electron in the lowest unoccupied molecular orbital (LUMO) of the acceptor and the hole in the highest occupied molecular orbital (HOMO) of the donor.[31−34] Then the electron−hole pairs could further efficiently dissociate into the free charge carriers that consequently contribute to the photocurrent.[35,36] Historically, it was empirically believed that sufficient frontier molecular orbital energy level offsets between donor and electron materials (including the HOMO offset $\Delta E_{HOMO(D-A)}$ and the LUMO offset $\Delta E_{LUMO(D-A)}$, which were typically ≥0.3 eV in the fullerene-based PSCs) are necessary to

Received: September 13, 2019
Published: January 6, 2020

https://dx.doi.org/10.1021/jacs.9b09939
J. Am. Chem. Soc. 2020, 142, 1465−1474

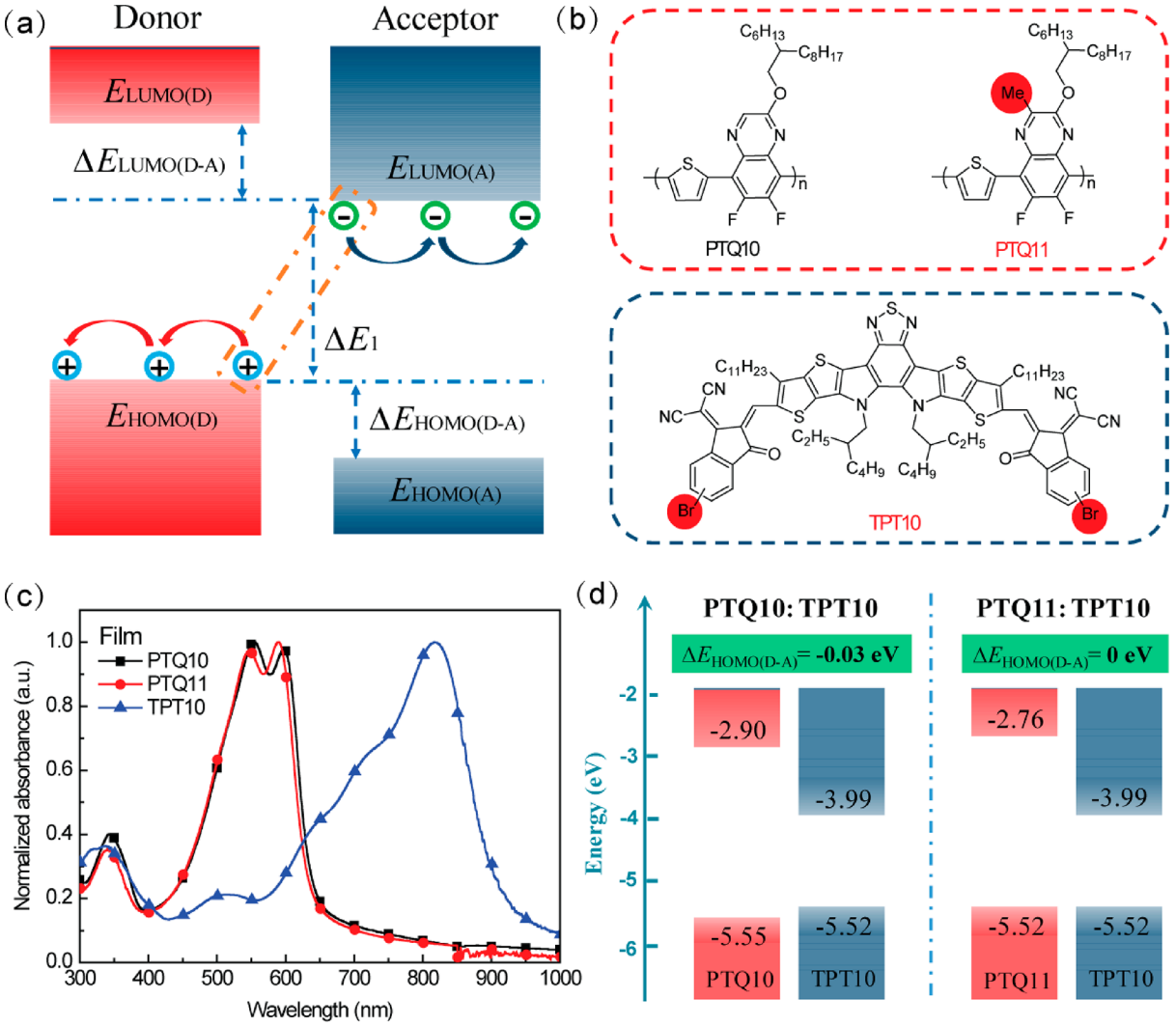

Figure 1. (a) Working mechanism diagram of charge separation at the donor−acceptor interfaces. (b) Molecular structures of polymer donors PTQ10 and PTQ11 and acceptor TPT10. (c) Normalized absorption spectra of polymer donors PTQ10 and PTQ11 and acceptor TPT10. (d) Energy level diagrams of PTQ10−TPT10 blend and PTQ11−TPT10 blend.

provide a driving force for fast and efficient charge separation in PSCs.[16,37,38] In recent years, due to the emergence of efficient n-OS acceptors, several works have demonstrated highly efficient PSCs with fast charge separation at HOMO offset smaller than 0.3 eV.[39−43] For example, Yan et al. reported a device (PffBT2T-TT−*O*-IDTBR) with a HOMO offset of 0.09 eV and a PCE of 10.4%.[39] Our group had reported a PSC (J71−ITIC) with a HOMO offset of 0.11 eV and a PCE of 11.4% in 2016.[17] And Chen et al. recently reported a device (PTQ10−HC-PCIC) with a HOMO offset of 0 eV and a PCE of 10.42%.[35] These phenomena have attracted more and more attention in theoretical studies of PSCs. Friend et al. suggest that the electron−hole pairs could delocalize to approximately 5 nm distance within a few femtoseconds at the D/A interface.[44,45] Hou et al. suggest that the different electrostatic potential (ESP) between the donor and acceptor results in an intermolecular electric field (IEF), which facilitates exciton dissociation.[46]

On the other hand, the distinct voltage loss (V_{loss}) from the difference between optical band gap (E_g) of the solar cell active layer and V_{oc} of the device ($V_{loss} = E_g/q - V_{oc}$) is one of the critical limitations for pursuing high efficiency PSCs.[47] To reduce V_{loss} and improve V_{oc} and PCE of the PSCs, one of the feasible methods is to increase the difference between LUMO energy level (E_{LUMO}) of the acceptor and HOMO energy level (E_{HOMO}) of the donor ($\Delta E_1 = E_{LUMO(A)} - E_{HOMO(D)}$), as the V_{oc} of PSCs is proportional to ΔE_1, which could be enlarged by up-shifting E_{LUMO} of the acceptor (reducing $\Delta E_{LUMO(D-A)}$) or down-shifting E_{HOMO} of donor (reducing $\Delta E_{HOMO(D-A)}$) (Figure 1a).[48] However, as mentioned above, it is unknown whether fast and efficient charge separation (contributing the large J_{sc}) can be achieved in a blend with small $\Delta E_{HOMO(D-A)}$ or $\Delta E_{LUMO(D-A)}$ because there are no related theories.

Recently, Zou et al. reported a high performance n-OS acceptor, Y6, that possesses a strong absorption and low band gap of 1.33 eV and demonstrated a high PCE of 15.7% in PSCs with Y6 as acceptor and conjugated polymer PM6 as donor.[11] Nevertheless, the relatively low-lying LUMO of −4.10 eV for Y6 limited the V_{oc} of the Y6-based PSCs. The low LUMO of Y6 should be related to the strong electron-affinity bifluorine substitution on its end group. In order to further reduce the energy loss and improve the V_{oc} of the acceptor, here we design and synthesize a new n-OS acceptor, TPT10 (Figure 1b), by introducing monobromine substitution instead of

https://dx.doi.org/10.1021/jacs.9b09939
J. Am. Chem. Soc. 2020, 142, 1465−1474

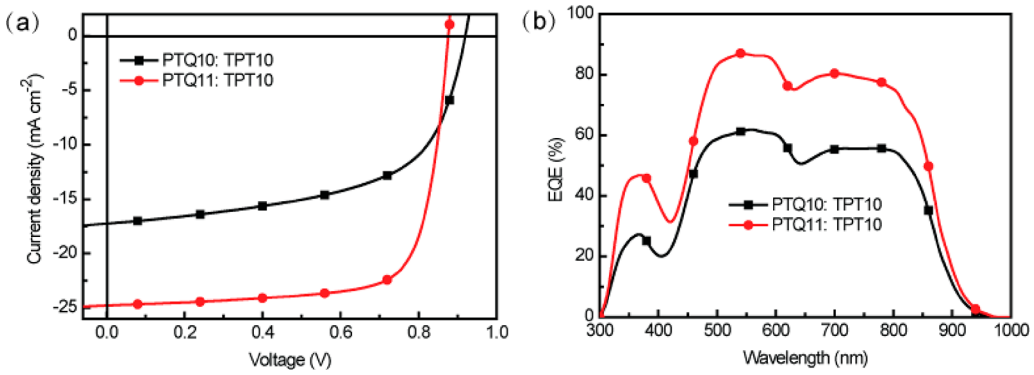

Figure 2. (a) $J-V$ curves of the inverted structured PSCs based on polymer−TPT10, under the illumination of AM 1.5G, 100 mW cm^{-2}. (b) EQE spectra of the corresponding PSCs based on polymer−TPT10.

bifluorine on the end group of Y6. TPT10 possesses an up-shifted E_{LUMO} of −3.99 eV and an E_{HOMO} of −5.52 eV due to the weaker electron-affinity of monobromine substituent of TPT10 in comparison with the bifluorine substituents of Y6. We first studied the photovoltaic performance of TPT10 by using our low cost conjugated polymer PTQ10[5] as donor. The PSC based on PTQ10−TPT10 displays a high V_{oc} of 0.92 V benefitting from the large difference between E_{LUMO} (−3.99 eV) of the acceptor TPT10 and E_{HOMO} (−5.55 eV) of the donor PTQ10. However, the device shows a lower PCE of 9.24% because of the lower J_{sc} and lower FF due to the negative $\Delta E_{HOMO(D-A)}$ (−0.03 eV), which results in the poor hole transfer from acceptor TPT10 to donor PTQ10. To overcome the poor hole transfer caused by the negative $\Delta E_{HOMO(D-A)}$, we introduced a methyl substituent onto the electron-deficient quinoxaline unit of PTQ10, considering that the methyl could slightly up-shift E_{HOMO} due to its weak electron-donating property. In addition, the small size of the methyl substituent will not disturb molecular packing of the polymer donor in the active layer. As expected, the resulting polymer, PTQ11, shows a slightly higher E_{HOMO} of −5.52 eV, which is identical to that of acceptor TPT10, and possesses stronger molecular crystallization and better hole transport capability than PTQ10. Encouragingly, the PTQ11−TPT10 based device with zero $\Delta E_{HOMO(D-A)}$ demonstrates a high PCE of 16.32% with the simultaneously enhanced V_{oc}, J_{sc}, and FF, which is one of the highest PCE values in single-junction PSCs.

RESULTS AND DISCUSSION

Materials Synthesis and Characterization. Molecular structures of polymer donors PTQ10 and PTQ11 and acceptor TPT10 are depicted in Figure 1b. The synthesis of acceptor TPT10 is similar to the reported works,[11,49] where the benzothiadiazole-based fused ring unit dithienothiophen[3,2-*b*]pyrrolobenzothiadiazole (TTPBT) is used as the electron-donating core and the monobromo-substituted 2-(3-oxo-2,3-dihydro-1*H*-inden-1-ylidene)malononitrile (INCN) is used as a strong electron-withdrawing terminal group. The synthetic details are described in Supporting Information. PTQ11 possesses the same advantages of simple molecular structure and low-cost synthesis as PTQ10,[5] and its detailed synthetic route and synthetic procedures are also described in the Supporting Information. PTQ10 is synthesized according to our previous work.[5] The number-average molecular weights (M_n) of PTQ10 and PTQ11 are measured to be 30.2 and 35.6 kDa with polydispersity index (PDI) of 1.6 and 2.1, respectively, measured by high temperature gel permeation chromatography (GPC), as listed in Table S1. The acceptor TPT10 and the two polymers possess good solubility in common organic solvents, such as chloroform and chlorobenzene, at room temperature.

Figure 1c shows the normalized UV−vis absorption spectra of the donor polymers PTQ10 and PTQ11 and acceptor TPT10 in their thin films, and their corresponding optical data are shown in Table S1. As we reported previously,[5] PTQ10 shows an absorption edge of 645 nm and an optical band gap of 1.92 eV. For the thin film, PTQ11 shows strong absorption in the range of 450 to 620 nm with the absorption edge located at 637 nm, which corresponds to an optical band gap of 1.95 eV. In comparison with PTQ10, PTQ11 shows slightly blue-shifted absorption. Both of the two polymers show well-defined absorption profiles with obvious absorption shoulder peaks, which can be ascribed to the vibronic band transitions. This feature indicates that the two polymers could possess molecular self-assembly aggregation and good charge transport capability in their blend films. For the acceptor TPT10 film, its absorption peak is located at 817 nm with an absorption edge at 910 nm corresponding to an optical band gap of 1.36 eV. The two polymers and acceptor TPT10 display complementary absorption in the range of 400 to 900 nm, which will benefit solar photon harvest thus increasing J_{sc} of the PSCs.

Cyclic voltammetry measurements with Ag/AgCl reference electrode are performed to estimate the electronic energy levels of the two polymers and acceptor TPT10 (Figure S1), and their E_{HOMO}/E_{LUMO} values are calculated from onset oxidation and onset reduction potentials ($\varphi_{ox}/\varphi_{red}$) according to the equation of $E_{HOMO/LUMO} = -e(\varphi_{ox/red} - \varphi_{Fc/Fc^+} + 4.80)$ eV, where the φ_{Fc/Fc^+} is measured to be 0.47 V vs Ag/AgCl reference electrode. The E_{HOMO}/E_{LUMO} values of PTQ10, PTQ11, and TPT10 are measured to be −5.55/−2.90, −5.52/−2.76, and −5.52/−3.99 eV, respectively (Figure 1d). As expected, the acceptor TPT10 possesses an up-shifted E_{LUMO} of −3.99 eV in comparison with Y6 owing to the weaker electron affinity of monobromine substituents in TPT10 compared with that of the bifluorine substituents in Y6, and the polymer PTQ11 also shows slightly up-shifted electronic energy levels (both E_{HOMO} and E_{LUMO}) due to the electron-donating methyl substitution on its quinoxaline unit. It is worth noting that the $\Delta E_{HOMO(D-A)}$ of the blend active layers of PTQ10−TPT10 and PTQ11−TPT10 are low values of −0.03 and 0 eV, respectively (Figure 1d). To confirm these razor-sharp $\Delta E_{HOMO(D-A)}$ values, we also measured E_{HOMO} of the two polymer donors (PTQ10 and PTQ11) and the acceptor TPT10 through ultraviolet photoelectron spectrosco-

https://dx.doi.org/10.1021/jacs.9b09939
J. Am. Chem. Soc. 2020, 142, 1465−1474

py (UPS). The HOMO energy level differences from the UPS results (see Figure S2) are consistent with those from the CV measurements, which show a $\Delta E_{HOMO(D-A)}$ value of −0.02 eV between PTQ10 and TPT10 and 0 eV between PTQ11 and TPT10. This result indicates that the PSCs based on them will show high V_{oc} but it will be a huge challenge to achieve fast and efficient charge separation by hole transfer of excitons of the acceptor in the corresponding devices.

Photovoltaic Properties. To investigate the photovoltaic properties of the PTQ10−TPT10 blend and the PTQ11−TPT10 blend with negative and zero $\Delta E_{HOMO(D-A)}$ values, respectively, here we fabricate the inverted PSCs with device structures of ITO (indium tin oxide)/ZnO/PTQ10−TPT10 or PTQ11−TPT10/MoO_3/Ag. As the polymers PTQ10 and PTQ11 have similar molecular structure and approximate molecular weight, the PSCs based on PTQ10 and PTQ11 have identical optimized device fabrication conditions including the donor/acceptor weight ratio of 1:1.2 with a total concentration of 18 mg/mL and with 0.5% 1-chloronaphthalene (1-CN) as additive in their chloroform solution (see Table S2 and Table S3), spin coating at 3000 rpm for 40 s with an active layer thickness of ca. 110 nm (see Table S4), and thermal annealing at 110 °C for 5 min (see Table S5). Figure 2a shows the current density−voltage ($J-V$) curves of the optimal devices based on PTQ10−TPT10 and PTQ11−TPT10 under the illumination of AM1.5G, 100 mW cm^{-2}, and the corresponding photovoltaic performance parameters are listed in Table 1.

Table 1. Photovoltaic Performance Parameters of the PSCs Based on Polymer−TPT10 under the Illumination of AM 1.5G, 100 mW cm^{-2}

devices	V_{oc} (V)	J_{sc} (mA cm^{-2})	FF (%)	PCE (%)
PTQ10−TPT10	0.92	17.25	58.2	9.24 (9.17 ± 0.04)[a]
PTQ11−TPT10	0.88	24.79	74.8	16.32 (16.09 ± 0.16)[a]

[a]The average values are calculated from 10 devices.

The PTQ10−TPT10 based device shows a high V_{oc} of 0.92 V (see Table 1), which should benefit from the higher-lying E_{LUMO} of the acceptor TPT10 and the low-lying E_{HOMO} of the polymer donor PTQ10. However, this device shows a lower PCE of 9.24% because of the low J_{sc} of 17.25 mA cm^{-2} and low FF of 58.2%, which should be ascribed to the poor charge carrier generation and transport in its blend due to the negative $\Delta E_{HOMO(D-A)}$ value between donor PTQ10 and acceptor TPT10. Importantly, the PSC based on PTQ10−TPT10 demonstrates an impressively high PCE of 16.32% with a higher V_{oc} of 0.88 V, a large J_{sc} of 24.79 mA cm^{-2}, and a high FF of 74.8%, despite the zero $\Delta E_{HOMO(D-A)}$ value between donor PTQ11 and acceptor TPT10. The efficiency of 16.32% is one of the highest PCE values among single-junction PSCs.

To confirm the photovoltaic data of the devices from $J-V$ measurements, we measure the external quantum efficiency (EQE) of the corresponding optimized devices; the results are shown in Figure 2b. It is found that the device based on PTQ10−TPT10 with negative $\Delta E_{HOMO(D-A)}$ exhibits poor photon response, thus resulting in low photoelectric conversion efficiency with a maximum EQE value of only 61.97%. In contrast, the PTQ11−TPT10 based device shows broad and strong photon response with high EQE values over 60% in the broad wavelength region from 450 to 850 nm even though the $\Delta E_{HOMO(D-A)}$ value between donor PTQ11 and acceptor TPT10 is zero, which means that high exciton dissociation efficiency and fast charge carrier transport are achieved in the PTQ11−TPT10 blend film. The current density values integrated from the EQE spectra under the AM1.5G spectrum are 16.78 mA cm^{-2} for the PTQ10−TPT10 based device and 23.75 mA cm^{-2} for the PTQ11−TPT10 based device, which are consistent with the J_{sc} values from $J-V$ curves within 5% mismatch, indicating the reliability of the measured photovoltaic data.

Exciton Dissociation and Charge Carrier Recombination Behavior. A PSC device that works highly efficiently requires the synergistic contributions of sunlight absorption, charge separation, charge carrier transport, and collection at electrodes, in which charge separation is a critical process. As mentioned above, the energy level offsets (both $\Delta E_{HOMO(D-A)}$ and $\Delta E_{LUMO(D-A)}$) between donor and acceptor are believed to provide the driving force for charge separation in PSCs. In order to investigate the exciton dissociation and charge transportation efficiencies of the PSCs based on PTQ10−TPT10 and PTQ11−TPT10 with negative and zero $\Delta E_{HOMO(D-A)}$, respectively, here we study the relationship between photocurrent density (J_{ph}) and effective voltage (V_{eff}) of the devices. J_{ph} is defined as $J_{ph} = J_L - J_D$, where J_L and J_D are the current densities of the devices under illumination and in the dark, respectively. V_{eff} is defined as $V_{eff} = V_0 - V_{bias}$, where V_0 is the voltage when J_{ph} is zero and V_{bias} is the applied voltage bias. Therefore, V_{eff} determines the electric field in the donor/acceptor blend films and thus affects the exciton dissociation and charge transport behavior. The charge carriers move quickly to the corresponding electrodes and J_{ph} reaches

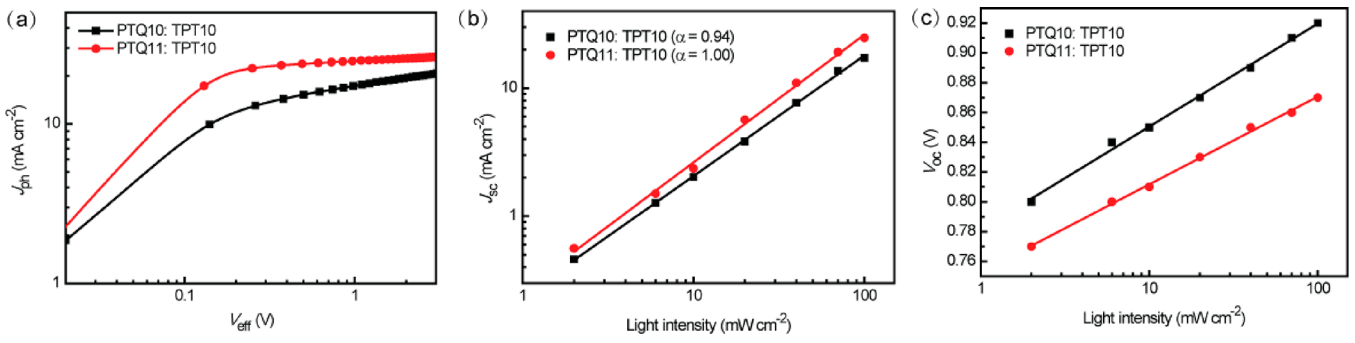

Figure 3. (a) J_{ph} versus V_{eff} of the devices based on polymer−TPT10. (b) Dependence of J_{sc} on P_{light} of the devices based on polymer−TPT10. (c) Dependence of V_{oc} on P_{light} of the devices based on polymer−TPT10.

https://dx.doi.org/10.1021/jacs.9b09939
J. Am. Chem. Soc. 2020, 142, 1465−1474

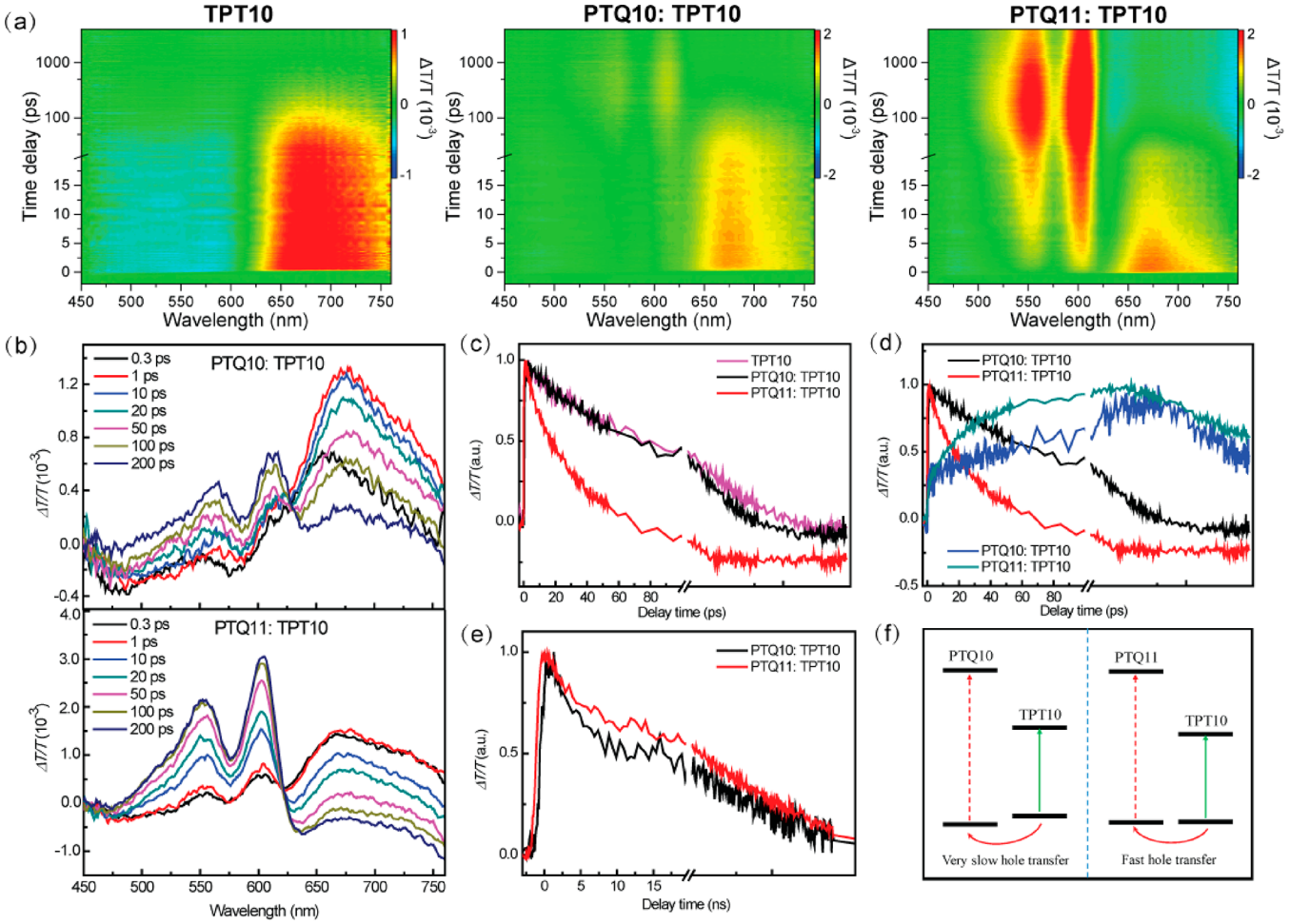

Figure 4. (a) Femtosecond-resolved TA signals recorded from the neat TPT10 film and the polymer−TPT10 blend films excited at 800 nm. (b) Femtosecond-resolved TA spectra from the polymer− TPT10 blend film excited at 800 nm at different delay times. (c) Femtosecond-resolved TA dynamic curves probed at 675 nm recorded from the neat TPT10 film and the polymer−TPT10 blend films excited at 800 nm. (d) Femtosecond-resolved TA dynamic curves probed at 675 nm (black for PTQ10−TPT10 and red for PTQ11−TPT10), 612 nm (blue for PTQ10−TPT10), and 602 nm (dark cyan for PTQ11−TPT10) recorded from the polymer−TPT10 blend film excited at 800 nm. (e) Nanosecond-resolved TA dynamic curves probed at 612 nm (PTQ10−TPT10) and 602 nm (PTQ11−TPT10) recorded from the polymer−TPT10 blend film excited by 532 nm. (f) Schematic diagram of the hole transfer process in the polymer−TPT10 blend.

saturation (J_{sat}) at a high V_{eff} ($V_{eff} \geq 2$ V), suggesting that all photogenerated carriers are extracted and collected with minimal recombination. Thus, the exciton dissociation probability of the PSCs can be calculated by J_{ph}/J_{sat}. For the device based on PTQ10−TPT10 with negative $\Delta E_{HOMO(D-A)}$ value, a low exciton dissociation probability of 88.8% is observed as shown in Figure 3a, which indicates the poor exciton dissociation behavior in the PTQ10−TPT10 blend film. However, the device based on methyl-substituted polymer donor PTQ11 and acceptor TPT10 shows a high exciton dissociation probability of 96.2% even though the $\Delta E_{HOMO(D-A)}$ value between PTQ11 and TPT10 is zero. This result indicates that fast and efficient exciton dissociation can occur in the n-OS acceptor-based PSCs with zero $\Delta E_{HOMO(D-A)}$, but the exciton dissociation is seriously restricted when $\Delta E_{HOMO(D-A)}$ reduces to negative values. The high exciton dissociation efficiency in the device based on PTQ11−TPT10 with zero $\Delta E_{HOMO(D-A)}$ could be due to the formation of the delocalized electron−hole pairs at the D/A interface[44,45] or the existence of an intermolecular electric field between the donor and acceptor owing to their different electrostatic potential (ESP),[46] which facilitates exciton dissociation. Moreover, the possibly high local charge carrier mobility at the D/A interfaces and the entropy contribution[50,51] from the high dimensional PTQ11 donor and TPT10 acceptor could also favor exciton dissociation.

Charge carrier recombination in the active layer of the PSCs is another critical issue that affects the free charge generation and transport. To understand the charge carrier recombination behavior of the PSCs, we study the dependence of J_{sc} and V_{oc} on light intensity (P_{light}). The relationship between J_{sc} and P_{light} can be depicted by the formula $J_{sc} \propto (P_{light})^{\alpha}$, where the α value indicates the degree of bimolecular recombination. The α value should be 1 when there is no bimolecular recombination in the blend active layer, and some bimolecular recombination exists when the α value is smaller than 1. Figure 3b shows the plots of log J_{sc} versus log P_{light}, and slope α values are 0.94 and 1.00 for the PSCs based on PTQ10−TPT10 and PTQ11−TPT10, respectively. The α value of 1.00 for the PTQ11−TPT10 based device indicates there is almost no bimolecular recombination in its active layer in spite of the zero $\Delta E_{HOMO(D-A)}$ between donor PTQ11 and acceptor TPT10. However, some bimolecular recombination occurs in the PTQ10−TPT10 blend with the negative $\Delta E_{HOMO(D-A)}$ value of −0.03 eV. On

https://dx.doi.org/10.1021/jacs.9b09939
J. Am. Chem. Soc. 2020, 142, 1465−1474

the other hand, if bimolecular recombination is the exclusive recombination form in the blend films, the slope of the fitting line of V_{oc} versus ln(P_{light}) should be kT/e (where e is the elementary charge, k is the Boltzmann constant and T is the Kelvin temperature). The plots of V_{oc} versus ln(P_{light}) of the two devices are shown in Figure 3c. The slopes of the fitting lines for the PSCs based on PTQ10−TPT10 and PTQ11−TPT10 are $1.20kT/e$ and $1.02kT/e$, respectively. The slope very close to kT/e for the PTQ11−TPT10 based device indicates that there are very few other recombination forms in its active layer, and the slope of $1.20kT/e$ for the PTQ10−TPT10 based device suggests that obvious recombination occurs in its active layer. The results of J_{sc} and V_{oc} dependence on P_{light} indicate that there is almost no charge carrier recombination in the PTQ11−TPT10 blend despite the zero $\Delta E_{HOMO(D-A)}$, which consequently results in a highly efficient PSC based on PTQ11−TPT10 with zero $\Delta E_{HOMO(D-A)}$ value.

Hole Transfer Dynamics. As mentioned above, it is likely that charge transfer (including electron transfer and hole transfer) in the PTQ10−TPT10 blend is strictly restricted due to the negative $\Delta E_{HOMO(D-A)}$; in contrast, this process in the PTQ11−TPT10 blend is highly fast and efficient even though $\Delta E_{HOMO(D-A)}$ is zero. To study the charge transfer dynamics of photoinduced carriers in these two blends, we perform transient absorption (TA) spectroscopy measurements to check the charge transfer details. As both blend active layers of PTQ10−TPT10 and PTQ11−TPT10 possess sufficient $\Delta E_{LUMO(D-A)}$ ($\Delta E_{LUMO(D-A)} > 1$ eV) for fast and efficient electron transfer from donor to acceptor, here we mainly focus our studies on the hole transfer process from acceptor to donor in the two blends. The primary absorption peaks for polymers PTQ10 and PTQ11 and acceptor TPT10 are well separated in spectral domain (Figure 1c), so we can study the spectral and temporal characteristics of the hole transfer dynamics with selected excitation. Here, a pump wavelength of 800 nm is selected to excite acceptor TPT10 only without exciting polymer donors PTQ10 and PTQ11 (Figure S3). The pump−probe experiments measure the pump-induced differential change of the probe transmission, $\Delta T/T = (T_{pump\text{-}on} - T_{pump\text{-}off})/T_{pump\text{-}off}$.

First, we perform femtosecond-resolved TA spectroscopy measurements to probe the hole transfer process in these two blends with a weak excitation density of ∼2 μJ cm^{-2} to avoid the effect of exciton−exciton annihilation. Figure 4a shows the color plots of TA spectra of the neat TPT10 film, PTQ10−TPT10 blend film, and PTQ11−TPT10 blend film with the 800 nm excitation. A bleaching signal located at 675 nm appears in the neat TPT10 film and the two blend films. This bleaching signal can be naturally ascribed to the transition of acceptor TPT10 from its absorption profile (Figure 1c). In addition, bleaching peaks in the shorter wavelength range (about 561 and 612 nm for PTQ10−TPT10 blend film and 552 and 602 nm for PTQ11−TPT10 blend film) are observed in the two blends, which should be attributed to the response signals of polymers. Figure 4b displays the TA spectra of the two blends with different delay times. Basically, the bleaching signals in the shorter wavelength range are built up with the decay of signal at 675 nm in both blends, suggesting the transfer of excitations from acceptor TPT10 to polymer donors. As the excitation photon energy at 800 nm is much smaller than that required for exciton absorption of the two polymers and the E_{LUMO} of acceptor TPT10 is much lower than that of the two polymer donors, those bleaching signals appearing in the shorter wavelength range can be assigned to the hole transfer from acceptor TPT10 to polymer donors instead of energy transfer or electron transfer processes. It is worth noting that very weak bleaching signals at 561 and 612 nm appear when the signal at 675 nm disappears in the PTQ10−TPT10 blend, which suggests that the hole transfer from acceptor TPT10 to donor PTQ10 is inappreciable. In contrast, conspicuous bleaching signals located at 552 and 602 nm appear as the signal at 675 nm disappears in the PTQ11−TPT10 blend, which indicates the fast and efficient hole transfer process from acceptor TPT10 to donor PTQ11.

Figure 4c compares the dynamic processes of the neat TPT10 film and two blend films probed at 675 nm on a normalized scale. It is found that the PTQ10−TPT10 blend film shows almost identical and slightly faster relaxation rate compared to the neat TPT10 film in the first 100 ps and later time, respectively, which means that there is only very little hole transfer from acceptor TPT10 to donor PTQ10 and this transfer process is very slow. In contrast, the relaxation rate of PTQ11−TPT10 blend films becomes dramatically faster with respect to the neat TPT10 film over the full time scale, indicating the presence of an efficient relaxation channel of hole transfer in the blend film. We quantified the early stage dynamics within 100 ps with a biexponential decay function. The lifetime parameters for the two components are about 86.4 and 86.4 ps, respectively, for the neat TPT10 film, and they markedly reduced to about 7.2 and 43.8 ps in the PTQ11−TPT10 blend film. Moreover, the onset of bleaching signals in the shorter wavelength range shows biexponential growth components with lifetime parameters of about 7.3 and 44.5 ps, respectively, for the PTQ11−TPT10 blend films (Figure 4d), confirming that the hole transfer from acceptor TPT10 to donor PTQ11 is the primary origin of the bleaching signals at the absorption band of polymer PTQ11.

We further performed nanosecond-resolved TA spectroscopy measurements to probe the lifetimes of charge separated (CS) states in the two blends (Figure 4e and Figure S4). The results show that both of the blends possess long enough CS state lifetime on the nanosecond scale, which suggests the existence of the long-lived dissociated excitons in the blend film for further electricity generation, and the PTQ11−TPT10 blend film exhibits a slower recombination process compared to the PTQ10−TPT10 blend film. With these results, we can briefly summarize that the hole transfer channel from acceptor TPT10 to donor PTQ10 with negative $\Delta E_{HOMO(D-A)}$ value is strictly restricted and the hole transfer process is very slow (Figure 4f); conversely, fast and efficient hole transfer are achieved in the PTQ11−TPT10 blend film even though $\Delta E_{HOMO(D-A)}$ is zero.

The hole mobility (μ_h) of the two devices is measured using the space charge limited current (SCLC) method with a hole-only device (ITO/PEDOT−PSS/PTQ10−TPT10 or PTQ11−TPT10/Au), and the measurement results are shown in Figure S5. As expected, the device based on PTQ11−TPT10 exhibits slightly higher μ_h of 0.97×10^{-4} cm^2 V^{-1} s^{-1} in comparison with the PTQ10−TPT10 based device (μ_h of 0.91×10^{-4} cm^2 V^{-1} s^{-1}). The improved hole mobility suggests better hole transport ability of the PTQ11−TPT10 based device, which is beneficial for obtaining large J_{sc} and high FF. This result together with the results mentioned above can collectively explain the remarkably enhanced photovoltaic performance of the PTQ11−TPT10 based device.

https://dx.doi.org/10.1021/jacs.9b09939
J. Am. Chem. Soc. 2020, 142, 1465−1474

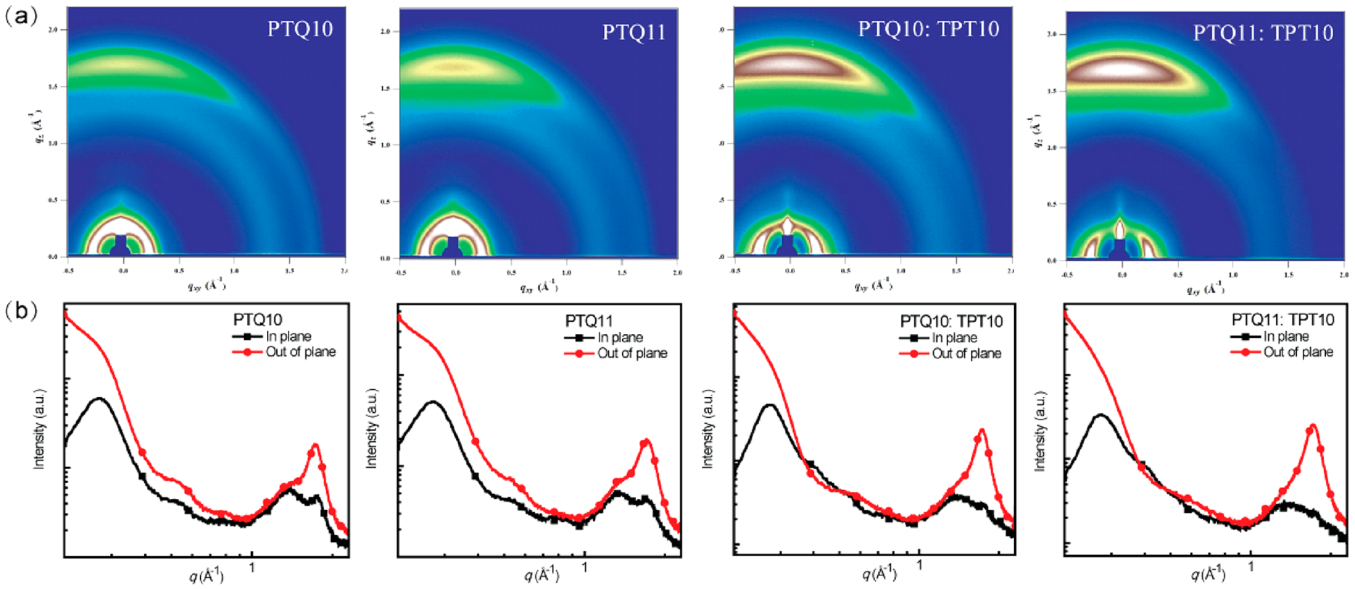

Figure 5. (a) GIWAXS images of the neat PTQ10 film, neat PTQ11 film, and polymer−TPT10 blend film. (b) Line cuts of the neat PTQ10 film, neat PTQ11 film, and polymer−TPT10 blend film.

Morphological Characterization. The aggregation morphology of the polymer donors and acceptors in the active layer is a critical factor to determine the photovoltaic performance of the PSCs. To probe the effect of methyl substitution of the polymer on the molecular ordering at the nanoscale, molecular crystallinity, and blend film morphology and thus the charge transport in the blend films, here we carry out grazing incident wide-angle X-ray diffraction (GIWAXS) measurements on the neat polymer films (neat PTQ10 film and neat PTQ11 film) and the blend films (PTQ10−TPT10 blend film and PTQ11−TPT10 blend film); the corresponding plots and images of GIWAXS measurements are shown in Figure 5. For the neat PTQ10 film, the $\pi-\pi$ stacking diffraction peak and laminar diffraction peak are located at 1.73 and 0.27 $Å^{-1}$ in the out-of-plane (OOP) direction, corresponding to a $\pi-\pi$ stacking distance of 3.63 Å and a lamellar distance of 23.44 Å respectively. And the neat PTQ11 film shows the $\pi-\pi$ stacking diffraction peak and laminar diffraction peak located at 1.72 and 0.27 $Å^{-1}$ in the OOP direction corresponding to a $\pi-\pi$ stacking distance of 3.65 Å and a lamellar distance of 23.44 Å, respectively. It is found that the two polymers show similar molecular packing features and preferential face-on molecular orientation with distinct $\pi-\pi$ stacking diffraction peaks in the vertical direction of substrate, which is believed to be beneficial for efficient charge transport. Moreover, it is worth noting that the PTQ11 film shows stronger $\pi-\pi$ stacking diffraction signal (Figure 5a) in comparison with the PTQ10 film, which suggests stronger molecular crystallinity of the polymer PTQ11 even though it shows a slightly enlarged $\pi-\pi$ stacking distance (3.65 Å for PTQ11 vs 3.63 Å for PTQ10) due to the increased steric hindrance from the methyl substitution. The stronger $\pi-\pi$ stacking feature indicates better hole transport capability of the polymer PTQ11, which is consisting with the mobility measurements. The GIWAXS results of the blend films demonstrate microstructural features with diffraction patterns contributed from individual polymer donor and acceptor components. Thus, just like the molecular stacking features of the neat polymer films and neat acceptor film (Figure S6), both the PTQ10−TPT10 blend film and the PTQ11−TPT10 blend film exhibit preferred face-on molecular packing orientation in the OOP direction, especially for the PTQ11−TPT10 blend film, indicating their better charge transport capability in the vertical direction of substrate. The results indicate that methyl substitution on the polymer PTQ10 slightly increases ordered packing behavior of the polymer chains, thus leading to better $\pi-\pi$ molecular stacking and higher crystalline characteristics of the polymer PTQ11, which consequently assists charge transport and improves photovoltaic performance of the device.

CONCLUSION

In conclusion, we designed and synthesized a new low band gap n-OS acceptor, TPT10, and a new low cost conjugated polymer donor, PTQ11. The acceptor TPT10 is a derivative of Y6 with monobromine substitution instead of difluorine substitution on its terminal groups, up-shifting E_{LUMO} of the acceptor to get higher V_{oc} of the PSCs, while the donor PTQ11 is a derivative of PTQ10 with methyl substitution on its quinoxaline unit for slightly up-shifting E_{HOMO} of the donor to match with the E_{HOMO} of TPT10 acceptor. The PSCs based on PTQ10−TPT10 display a high V_{oc} of 0.92 V benefitting from the higher-lying E_{LUMO} of −3.99 eV of TPT10 acceptor and the lower-lying E_{HOMO} of PTQ10 polymer donor, but a lower PCE of 9.24% due to the negative $\Delta E_{HOMO(D-A)}$ (−0.03 eV) between the PTQ10 donor and the TPT10 acceptor. Interestingly, the TPT10-based PSC with PTQ11 as donor shows a high PCE of 16.32% with a higher V_{oc} of 0.88 V, a larger J_{sc} of 24.79 mA cm^{-2}, and a higher FF of 74.8%, even with the zero $\Delta E_{HOMO(D-A)}$ value between donor PTQ11 and acceptor TPT10. The excellent photovoltaic performance of the PTQ11−TPT10-based PSC is explained by studies of morphology analysis and TA spectroscopy measurements. PTQ11 shows stronger molecular crystallization and better hole transport capability than PTQ10. Moreover, the PSC based on PTQ11−TPT10 shows highly efficient exciton dissociation and hole transfer despite the zero $\Delta E_{HOMO(D-A)}$. Overall, this work suggests that PSCs with zero $\Delta E_{HOMO(D-A)}$

https://dx.doi.org/10.1021/jacs.9b09939
J. Am. Chem. Soc. 2020, 142, 1465−1474

could possess efficient hole transfer and high PCE, which is highly valuable for further understanding the charge transfer process in PSCs and provides a valid methodology to further improve the PCE of PSCs.

■ ASSOCIATED CONTENT

Supporting Information

The Supporting Information is available free of charge at https://pubs.acs.org/doi/10.1021/jacs.9b09939.

Details of materials and synthesis, general characterization, device fabrication and characterization, cyclic voltammograms of the polymers and acceptor, fs-resolved and ns-resolved TA signal spectra, hole mobility from SCLC method, and GIWAXS image and plots of the neat PTQ11 film (PDF)

■ AUTHOR INFORMATION

Corresponding Author

Yongfang Li − *Institute of Chemistry, Chinese Academy of Sciences, Beijing, China, University of Chinese Academy of Sciences, Beijing, China, and Soochow University, Suzhou, China;* orcid.org/0000-0002-2565-2748; Email: liyf@iccas.ac.cn

Other Authors

Chenkai Sun − *Institute of Chemistry, Chinese Academy of Sciences, Beijing, China, and University of Chinese Academy of Sciences, Beijing, China*

Shucheng Qin − *Institute of Chemistry, Chinese Academy of Sciences, Beijing, China, and University of Chinese Academy of Sciences, Beijing, China*

Rui Wang − *Nanjing University, Nanjing, China*

Shanshan Chen − *Chongqing University, Chongqing, China, and Ulsan National Institute of Science and Technology (UNIST), Ulsan, Republic of Korea*

Fei Pan − *Institute of Chemistry, Chinese Academy of Sciences, Beijing, China, and University of Chinese Academy of Sciences, Beijing, China*

Beibei Qiu − *Institute of Chemistry, Chinese Academy of Sciences, Beijing, China, and University of Chinese Academy of Sciences, Beijing, China;* orcid.org/0000-0001-5288-5152

Ziya Shang − *Institute of Chemistry, Chinese Academy of Sciences, Beijing, China, and University of Chinese Academy of Sciences, Beijing, China*

Lei Meng − *Institute of Chemistry, Chinese Academy of Sciences, Beijing, China*

Chunfeng Zhang − *Nanjing University, Nanjing, China;* orcid.org/0000-0001-9030-5606

Min Xiao − *Nanjing University, Nanjing, China*

Changduk Yang − *Ulsan National Institute of Science and Technology (UNIST), Ulsan, Republic of Korea;* orcid.org/0000-0001-7452-4681

Complete contact information is available at: https://pubs.acs.org/10.1021/jacs.9b09939

Author Contributions

$^{\nabla}$C.S. and S.Q. contributed equally to this work.

Notes

The authors declare no competing financial interest.

■ ACKNOWLEDGMENTS

This work is supported by National Natural Science Foundation of China (Nos. 91633301, 21734008, and 51820105003) and the Basic and Applied Basic Research Major Program of Guangdong Province (No. 2019B030302007).

■ REFERENCES

(1) Yu, G.; Gao, J.; Hummelen, J. C.; Wudl, F.; Heeger, A. J. Polymer Photovoltaic Cells: Enhanced Efficiencies via a Network of Internal Donor-Acceptor Heterojunctions. *Science* **1995**, *270*, 1789.

(2) Liu, J.; Chen, S.; Qian, D.; Gautam, B.; Yang, G.; Zhao, J.; Bergqvist, J.; Zhang, F.; Ma, W.; Ade, H.; Inganäs, O.; Gundogdu, K.; Gao, F.; Yan, H. Fast Charge Separation in a Non-Fullerene Organic Solar Cell with a Small Driving Force. *Nat. Energy* **2016**, *1*, 16089.

(3) Li, Y. Molecular Design of Photovoltaic Materials for Polymer Solar Cells: Toward Suitable Electronic Energy Levels and Broad Absorption. *Acc. Chem. Res.* **2012**, *45*, 723.

(4) Li, G.; Zhu, R.; Yang, Y. Polymer Solar Cells. *Nat. Photonics* **2012**, *6*, 153.

(5) Sun, C.; Pan, F.; Bin, H.; Zhang, J.; Xue, L.; Qiu, B.; Wei, Z.; Zhang, Z.-G.; Li, Y. A Low Cost and High Performance Polymer Donor Material for Polymer Solar Cells. *Nat. Commun.* **2018**, *9*, 743.

(6) Li, X.; Pan, F.; Sun, C.; Zhang, M.; Wang, Z.; Du, J.; Wang, J.; Xiao, M.; Xue, L.; Zhang, Z.-G.; Zhang, C.; Liu, F.; Li, Y. Simplified Synthetic Routes for Low Cost and High Photovoltaic Performance *n*-Type Organic Semiconductor Acceptors. *Nat. Commun.* **2019**, *10*, 519.

(7) Cheng, P.; Li, G.; Zhan, X.; Yang, Y. Next-Generation Organic PhotovoltaicsBased on Non-Fullerene Acceptors. *Nat. Photonics* **2018**, *12*, 131.

(8) Li, G.; Shrotriya, V.; Huang, J.; Yao, Y.; Moriarty, T.; Emery, K.; Yang, Y. High-Efficiency Solution Processable Polymer Photovoltaic Cells by Self-Organization of Polymer Blends. *Nat. Mater.* **2005**, *4*, 864.

(9) Meng, X.; Hu, X.; Yang, X.; Yin, J.; Wang, Q.; Huang, L.; Yu, Z.; Hu, T.; Tan, L.; Zhou, W.; Chen, Y. Roll-to-Roll Printing of Meter-Scale Composite Transparent Electrodes with Optimized Mechanical and Optical Properties for Photoelectronics. *ACS Appl. Mater. Interfaces* **2018**, *10*, 8917.

(10) Sun, R.; Guo, J.; Sun, C.; Wang, T.; Luo, Z.; Zhang, Z.; Jiao, X.; Tang, W.; Yang, C.; Li, Y.; Min, J. A Universal Layer-by-Layer Solution-ProcessingApproach for Efficient Non-Fullerene Organic SolarCells. *Energy Environ. Sci.* **2019**, *12*, 384.

(11) Yuan, J.; Zhang, Y.; Zhou, L.; Zhang, G.; Yip, H.-L.; Lau, T.-K.; Lu, X.; Zhu, C.; Peng, H.; Johnson, P. A.; Leclerc, M.; Cao, Y.; Ulanski, J.; Li, Y.; Zou, Y. Single-Junction Organic Solar Cell with over15% Efficiency Using Fused-Ring Acceptorwith Electron-Deficient Core. *Joule* **2019**, *3*, 1140.

(12) Xu, X.; Feng, K.; Bi, Z.; Ma, W.; Zhang, G.; Peng, Q. Single-Junction Polymer Solar Cells with 16.35% Efficiency Enabled by a Platinum(II) Complexation Strategy. *Adv. Mater.* **2019**, *31*, 1901872.

(13) Cui, Y.; Yao, H.; Zhang, J.; Zhang, T.; Wang, Y.; Hong, L.; Xian, K.; Xu, B.; Zhang, S.; Peng, J.; Wei, Z.; Gao, F.; Hou, J. Over 16% Efficiency Organic Photovoltaic Cells Enabled by a Chlorinated Acceptor with Increased Open-Circuit Voltages. *Nat. Commun.* **2019**, *10*, 2515.

(14) Kim, Y.; Cook, S.; Tuladhar, S. M.; Choulis, S. A.; Nelson, J.; Durrant, J. R.; Bradley, D. D. C.; Giles, M.; McCulloch, I.; Ha, C.-S.; Ree, M. A Strong Regioregularity Effect in Self-Organizing Conjugated Polymer Films and High-Efficiency Polythiophene: Fullerene Solar Cells. *Nat. Mater.* **2006**, *5*, 197.

(15) Huo, L.; Zhang, S.; Guo, X.; Xu, F.; Li, Y.; Hou, J. Replacing Alkoxy Groups with Alkylthienyl Groups: A Feasible Approach to

Improve the Properties of Photovoltaic Polymers. *Angew. Chem., Int. Ed.* **2011**, *50*, 9697.
(16) Zhao, J.; Li, Y.; Yang, G.; Jiang, K.; Lin, H.; Ade, H.; Ma, W.; Yan, H. Efficient Organic Solar Cells Processed from Hydrocarbon Solvents. *Nat. Energy* **2016**, *1*, 15027.
(17) Bin, H.; Gao, L.; Zhang, Z.-G.; Yang, Y.; Zhang, Y.; Zhang, C.; Chen, S.; Xue, L.; Yang, C.; Xiao, M.; Li, Y. 11.4% Efficiency Non-Fullerene Polymer Solar Cellswith Trialkylsilyl Substituted 2D-Conjugated Polymer as Donor. *Nat. Commun.* **2016**, *7*, 13651.
(18) He, Y.; Chen, H.-Y.; Hou, J.; Li, Y. Indene-C_{60}Bisadduct: A New Acceptor for High-PerformancePolymer Solar Cells. *J. Am. Chem. Soc.* **2010**, *132*, 1377.
(19) Lin, Y.; Wang, J.; Zhang, Z.-Z.; Bai, H.; Li, Y.; Zhu, D.; Zhan, X. An Electron Acceptor Challenging Fullerenes for Efficient Polymer Solar Cells. *Adv. Mater.* **2015**, *27*, 1170.
(20) Fan, Q.; Su, W.; Wang, Y.; Guo, B.; Jiang, Y.; Guo, X.; Liu, F.; Russell, T. P.; Zhang, M.; Li, Y. Synergistic Effect of Fluorination on Both Donor and Acceptor Materials for High Performance Non-Fullerene Polymer Solar Cells with 13.5% Eficiency. *Sci. China: Chem.* **2018**, *61*, 531.
(21) Brabec, C. J.; Shaheen, S. E.; Winder, C.; Sariciftci, N. S.; Denk, P. Effect of LiF/Metal Electrodes on The Performance of Plastic Solar Cells. *Appl. Phys. Lett.* **2002**, *80*, 1288.
(22) Kim, J. Y.; Kim, S. H.; Lee, H.-H.; Lee, K.; Ma, W.; Gong, X.; Heeger, A. J. New Architecture for High-Efficiency Polymer Photovoltaic Cells Using Solution-Based Titanium Oxide as an Optical Spacer. *Adv. Mater.* **2006**, *18*, 572.
(23) He, Z.; Zhong, C.; Huang, X.; Wong, W.-Y.; Wu, H.; Chen, L.; Su, S.; Cao, Y. Simultaneous Enhancement of Open-Circuit Voltage, Short-Circuit Current Density, and Fill Factor in Polymer Solar Cells. *Adv. Mater.* **2011**, *23*, 4636.
(24) Page, Z. A.; Liu, Y.; Duzhko, V. V.; Russell, T. P.; Emrick, T. Fulleropyrrolidine Interlayers: Tailoring Electrodes to Raise Organic Solar Cell Efficiency. *Science* **2014**, *346*, 441.
(25) Zhang, Z.-G.; Qi, B.; Jin, Z.; Chi, D.; Qi, Z.; Li, Y.; Wang, J. Perylene Diimides: A Thickness-Insensitive CathodeInterlayer for High Performance Polymer Solar Cells. *Energy Environ. Sci.* **2014**, *7*, 1966.
(26) Campoy-Quiles, M.; Ferenczi, T.; Agostinelli, T.; Etchegoin, P. G.; Kim, Y.; Anthopoulos, T. D.; Stavrinou, P. N.; Bradley, D. D. C.; Nelson, J. Morphology Evolution via Self-Organization and Lateral and Vertical Diffusion in Polymer: Fullerene Solar Cell Blends. *Nat. Mater.* **2008**, *7*, 158.
(27) Ye, L.; Zhang, S.; Ma, W.; Fan, B.; Guo, X.; Huang, Y.; Ade, H.; Hou, J. From Binary to Ternary Solvent: Morphology Fine-Tuningof D/A Blends in PDPP3T-based Polymer Solar Cells. *Adv. Mater.* **2012**, *24*, 6335.
(28) Zhou, N.; Facchetti, A. Naphthalenediimide (NDI) Polymers for All-Polymer Photovoltaics. *Mater. Today* **2018**, *21*, 377.
(29) Zhang, Z.-G.; Li, Y. F. Side-Chain Engineering of High Efficiency Conjugated Polymer Photovoltaic Materials. *Sci. China: Chem.* **2015**, *58*, 192.
(30) Timalsina, A.; Hartnett, P. E.; Melkonyan, F. S.; Strzalka, J.; Reddy, V. S.; Facchetti, A.; Wasielewski, M. R.; Marks, T. J. New Donor Polymer with Tetrafluorinated Blocks for Enhanced Performance in Perylenediimide-Based Solar Cells. *J. Mater. Chem. A* **2017**, *5*, 5351.
(31) Bakulin, A. A.; Rao, A.; Pavelyev, V. G.; van Loosdrecht, P. H. M.; Pshenichnikov, M. S.; Niedzialek, D.; Cornil, J.; Beljonne, D.; Friend, R. H. The Role of Driving Energy and Delocalized States for Charge Separation in Organic Semiconductors. *Science* **2012**, *335*, 1340.
(32) Tang, A.; Xiao, B.; Wang, Y.; Gao, F.; Tajima, K.; Bin, H.; Zhang, Z.-G.; Li, Y.; Wei, Z.; Zhou, E. Simultaneously Achieved High Open-Circuit Voltage and Efficient Charge Generation by Fine-Tuning Charge-Transfer Driving Force in Nonfullerene Polymer Solar Cells. *Adv. Funct. Mater.* **2018**, *28*, 1704507.
(33) Sini, G.; Schubert, M.; Risko, C.; Roland, S.; Lee, O. P.; Chen, Z.; Richter, T. V.; Dolfen, D.; Coropceanu, V.; Ludwigs, S.; Scherf, U.; Facchetti, A.; Fréchet, J. M. J.; Neher, D. On the Molecular Origin of Charge Separation at the Donor−Acceptor Interface. *Adv. Energy Mater.* **2018**, *8*, 1702232.
(34) Menke, S. M.; Ran, N. A.; Bazan, G. C.; Friend, R. H. Understanding Energy Loss in Organic Solar Cells: Toward a New Efficiency Regime. *Joule* **2018**, *2*, 25.
(35) Li, S.; Zhan, L.; Sun, C.; Zhu, H.; Zhou, G.; Yang, W.; Shi, M.; Li, C.-Z.; Hou, J.; Li, Y.; Chen, H. Highly Efficient Fullerene-Free Organic Solar Cells Operate at Near Zero Highest Occupied Molecular Orbital Offset. *J. Am. Chem. Soc.* **2019**, *141*, 3073.
(36) Xue, L.; Yang, Y.; Xu, J.; Zhang, C.; Bin, H.; Zhang, Z.-G.; Qiu, B.; Li, X.; Sun, C.; Gao, L.; Yao, J.; Chen, X.; Yang, Y.; Xiao, M.; Li, Y. Side Chain Engineering on Medium Bandgap Copolymersto Suppress Triplet Formation for High-Efficiency Polymer Solar Cells. *Adv. Mater.* **2017**, *29*, 1703344.
(37) Chen, J.-D.; Cui, C.; Li, Y.-Q.; Zhou, L.; Ou, Q.-D.; Li, C.; Li, Y.; Tang, J.-X. Single-Junction Polymer Solar Cells Exceeding 10% Power Conversion Efficiency. *Adv. Mater.* **2015**, *27*, 1035.
(38) Vohra, V.; Kawashima, K.; Kakara, T.; Koganezawa, T.; Osaka, I.; Takimiya, K.; Murata, H. Efficient Inverted Polymer Solar Cells Employing Favorable Molecular orientation. *Nat. Photonics* **2015**, *9*, 403.
(39) Chen, S.; Wang, Y.; Zhang, L.; Zhao, J.; Chen, Y.; Zhu, D.; Yao, H.; Zhang, G.; Ma, W.; Friend, R. H.; Chow, P. C. Y.; Gao, F.; Yan, H. Efficient Nonfullerene Organic Solar Cells with Small Driving Forces for Both Hole and Electron Transfer. *Adv. Mater.* **2018**, *30*, 1804215.
(40) Bin, H.; Yang, Y.; Peng, Z.; Ye, L.; Yao, J.; Zhong, L.; Sun, C.; Gao, L.; Huang, H.; Li, X.; Qiu, B.; Xue, L.; Zhang, Z.-G.; Ade, H.; Li, Y. Effect of Alkylsilyl Side-Chain Structure on Photovoltaic Properties of Conjugated Polymer Donors. *Adv. Energy Mater.* **2018**, *8*, 1702324.
(41) Bin, H.; Zhang, Z.-G.; Gao, L.; Chen, S.; Zhong, L.; Xue, L.; Yang, C.; Li, Y. Non-Fullerene Polymer Solar Cells Based on Alkylthio and Fluorine Substituted 2D-Conjugated Polymers Reach 9.5% Efficiency. *J. Am. Chem. Soc.* **2016**, *138*, 4657.
(42) Zhang, H.; Li, S.; Xu, B.; Yao, H.; Yang, B.; Hou, J. Fullerene-Free Polymer Solar Cell Based on a Polythiophene Derivative with an Unprecedented Energy Loss of Less Than 0.5 eV. *J. Mater. Chem. A* **2016**, *4*, 18043.
(43) Zhang, Z.; Liu, W.; Rehman, T.; Ju, H.-X.; Mai, J.; Lu, X.; Shi, M.; Zhu, J.; Li, C.-Z.; Chen, H. Energy-Level Modulation of Non-Fullerene Acceptors to Achieve High-Efficiency Polymer Solar Cells at a Diminished Energy Offset. *J. Mater. Chem. A* **2017**, *5*, 9649.
(44) Gelinas, S.; Rao, A.; Kumar, A.; Smith, S. L.; Chin, A. W.; Clark, J.; van der Poll, T. S.; Bazan, G. C.; Friend, R. H. Ultrafast Long-Range Charge Separation in Organic Semiconductor Photovoltaic Diodes. *Science* **2014**, *343*, 512.
(45) Jakowetz, A. C.; Böhm, M. L.; Sadhanala, A.; Huettner, S.; Rao, A.; Friend, R. H. Visualizing Excitations at Buried Heterojunctions in Organic Semiconductor Blends. *Nat. Mater.* **2017**, *16*, 551.
(46) Yao, H.; Cui, Y.; Qian, D.; Ponseca, C. S., Jr.; Honarfar, A.; Xu, Y.; Xin, J.; Chen, Z.; Hong, L.; Gao, B.; Yu, R.; Zu, Y.; Ma, W.; Chabera, P.; Pullerits, T.; Yartsev, A.; Gao, F.; Hou, J. 14.7% Efficiency Organic Photovoltaic Cells Enabled by Active Materials with a Large Electrostatic Potential Difference. *J. Am. Chem. Soc.* **2019**, *141*, 7743.
(47) Wang, Y.; Qian, D.; Cui, Y.; Zhang, H.; Hou, J.; Vandewal, K.; Kirchartz, T.; Gao, F. Optical Gaps of Organic Solar Cells as a Referencefor Comparing Voltage Losses. *Adv. Energy Mater.* **2018**, *8*, 1801352.
(48) Menke, S. M.; Sadhanala, A.; Nikolka, M.; Ran, N. A.; Ravva, M. K.; Abdel-Azeim, S.; Stern, H. L.; Wang, M.; Sirringhaus, H.; Nguyen, T.-Q.; Brédas, J.-L.; Bazan, G. C.; Friend, R. H. Limits for Recombination in a Low Energy Loss Organic Heterojunction. *ACS Nano* **2016**, *10*, 10736.
(49) Zhang, Z.-G.; Yang, Y.; Yao, J.; Xue, L.; Chen, S.; Li, X.; Morrison, W.; Yang, C.; Li, Y. Constructing a Strongly Absorbing Low-Bandgap Polymer Acceptorfor High-Performance All-Polymer Solar Cells. *Angew. Chem., Int. Ed.* **2017**, *56*, 13503.

https://dx.doi.org/10.1021/jacs.9b09939
J. Am. Chem. Soc. 2020, 142, 1465−1474

(50) Clarke, T. M.; Durrant, J. R. Charge Photogeneration in Organic Solar Cells. *Chem. Rev.* **2010**, *110*, 6736−6767.
(51) Gregg, B. A. Entropy of Charge Separation in Organic Photovoltaic Cells: The Benefit of Higher Dimensionality. *J. Phys. Chem. Lett.* **2011**, *2*, 3013−3015.

https://dx.doi.org/10.1021/jacs.9b09939
J. Am. Chem. Soc. 2020, 142, 1465−1474